ASME Journal of Mechanisms and Robotics
Online journal at:
https://asmedigitalcollection.asme.org/mechanismsrobotics

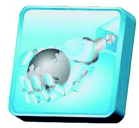

Seyoung Kim[1]
Advanced Robotics Research Center,
Korea Institute of Machinery & Materials (KIMM),
Daejeon 34103, South Korea
e-mail: seyoungkim@kimm.re.kr

Jongcheon Park
Advanced Robotics Research Center,
Korea Institute of Machinery & Materials (KIMM),
Daejeon 34103, South Korea
e-mail: jcpark@kimm.re.kr

Hyunho Jeong
Korea Advanced Institute of Science and Technology (KAIST),
Daejeon 34141, South Korea
e-mail: hyunho.jeong@kaist.ac.kr

Hyunmok Jung
Advanced Robotics Research Center,
Korea Institute of Machinery & Materials (KIMM),
Daejeon 34103, South Korea
e-mail: gusahr79@kimm.re.kr

Cheolhoon Park
Advanced Robotics Research Center,
Korea Institute of Machinery & Materials (KIMM),
Daejeon 34103, South Korea
e-mail: parkch@kimm.re.kr

Design of a Bistable Inertial Clutch for a Passive-Elastic Ankle Exoskeleton

Unpowered ankle exoskeletons are advantageous over powered ankle exoskeletons owing to their low weight. However, passive ankle exoskeletons without force transmission control can cause discomfort in certain situations. In this study, we designed a bistable inertial clutch that controls spring force transmission using phase-specific inertial forces generated by foot movement during walking. It features a ratchet–pawl mechanism, dual passive springs, and an inertial weight to switch between engaged and disengaged states. The design facilitated the timely storage and release of elastic energy at a certain walking speed and ensured that interruptions to the slow movement of exoskeleton wearers were minimal. We determined the optimal mass of an inertial weight of the clutch using an optimization method that synchronizes the clutch motion with changes in the walking phase. Eight subjects walked on a treadmill at five speeds (0.8–1.6 m/s), and foot angle, heel acceleration, and foot pressure were measured using a custom-made walking boot. Optimal inertial weights for each speed were obtained via a nonlinear optimization algorithm that minimized the least-squares error between foot pressure data and simulated clutch switching. Pilot testing showed that the clutch with the optimal weight for 1.2 m/s began switching between engagement and disengagement once the treadmill speed exceeded 1.2 m/s, as predicted. Thus, the clutch operated in sync with the stance and swing phases at sufficient speeds and remained stationary during low-acceleration leg movements. [DOI: 10.1115/1.4070415]

Keywords: bistable inertial clutch, ankle exoskeleton, inertial force, elastic energy, optimization, compact equipment development, mechanisms and robots, theoretical and computational kinematics, wearable devices

1 Introduction

Although powered ankle exoskeletons have successfully reduced the metabolic cost of human walking [1–4], unpowered ankle exoskeletons have a definitive advantage over powered ankle exoskeletons from a weight perspective because the passive working system does not require installed actuating modules and batteries. For instance, powered exoskeletons that use electric motors and leaf springs weigh over 4.0 kg [5–7] (including a battery pack and controller unit); powered soft exoskeletons that use motorized Bowden cables weigh approximately 4.0 kg [8]. The additional mass of the battery pack and the controller unit, placed at the waist and/or back, causes discomfort and fatigue, even while standing still or performing movements other than walking. In contrast, most unpowered exoskeletons weigh less than 2.0 kg [9–14].

The performance of unpowered ankle exoskeletons that assist ankle plantarflexion during walking cannot be maximized via lightweight alone. Simple and lightweight spring-loaded ankle exoskeletons (without batteries and controllers) that mimic the function of the Achilles tendon and ligaments passively support ankle push-off during simple locomotor movements (e.g., walking, jumping, hopping, and postural control) [9,15–17]. However, passive ankle exoskeletons without force transmission control can cause discomfort in certain situations, such as ankle motion in the aerial phase, because these devices increase the stiffness of the ankle–foot ligaments during ankle dorsiflexion in any leg movement [9,15]. Additionally, it is also difficult for the ankle exoskeletons to utilize a larger range of motion for elastic energy capture during the stance phase of walking.

Mechanical clutches have been developed to ensure timely ankle plantarflexion assistance during walking and to reduce discomfort in other leg movements. During the stance phase, the clutch is engaged and the assistance spring stretches and recoils, whereas during the swing phase, the clutch disengages to allow ankle dorsiflexion with only a small resistance [10,13]. To achieve such timely engagement and disengagement, existing mechanical clutches can be broadly classified into two categories based on their operating principle. The first is a kinematics-based approach that uses a

[1]Corresponding author.

Contributed by the Mechanisms and Robotics Committee of ASME for publication in the Journal of Mechanisms and Robotics. Manuscript received October 31, 2024; final manuscript received October 20, 2025; published online December 15, 2025. Assoc. Editor: Hao Su.

 Copyright © 2025 by ASME

specific joint angle, typically the angle of the ankle, as a trigger threshold. The pioneering kinematics-based approach employs an intuitive design in which a ratchet–pawl gear mechanism is triggered by the ankle angle [13,18–20]. This ratchet–pawl approach is advantageous for creating lightweight, purely mechanical systems. However, the performance of this approach is typically optimized for a specific walking speed, meaning that its effectiveness can decrease at other speeds and may require user-specific tuning [21]. To overcome these mechanical limitations, electronically controlled methods, such as electroadhesive clutches, have also been proposed [22]. The second is a kinetics-based approach that leverages the ground reaction force to trigger the clutch. This principle was initially demonstrated using force sensors to detect load changes [23] and was later implemented in purely mechanical forms, such as the sole-integrated triggers [24,25] or the body-weight-actuated friction mechanisms [10]. While this approach offers robust performance across diverse walking conditions, the requisite trigger structures can add complexity and mass to the system, potentially offsetting the assistive benefits [26]. Ultimately, both approaches share a common limitation: they rely on predefined kinematic conditions or external sensing, rather than adapting naturally to the dynamic changes that occur across different walking speeds.

In this study, we considered the inertial forces due to foot movement as the driving forces for clutch ON–OFF motion to minimize interruption to any slow movement of wearers, as well as for the timely storage and release of elastic energy at a certain walking speed. The concept originates from the inertial locking mechanism used in automotive seatbelt retractors [27,28]. In a crash or other rapid deceleration, this mechanism prevents further belt extension, thereby keeping the occupant securely restrained. We posit that the same principle can inform a clutch design for ankle exoskeletons. During walking, the foot naturally undergoes repeated deceleration, most notably at the onset and termination of the swing phase, creating an opportunity for an acceleration-sensitive clutch to passively engage and disengage in synchrony with gait dynamics. Such a bio-inspired clutch could reduce control complexity while enhancing energy efficiency and user safety. Accordingly, we designed a novel bistable inertial clutch that can operate synchronously with the stance and swing phases of walking when the walking speed reaches a certain threshold and beyond. Moreover, the clutch remains stationary if the acceleration or deceleration during leg movement is minimal. For better synchronization, the inertial weight added to the clutch was selected theoretically via an optimization strategy that minimized the least-squares error between the walking data and the clutch model simulation.

2 Methods

2.1 Mechanical Design and Mechanism of the Bistable Inertial Clutch. A bistable inertial clutch features a ratchet–pawl mechanism, dual passive springs, and an inertial weight to switch between engaged and disengaged states (Fig. 1). The two parallel springs help the clutch operate in synchrony with the stance and swing phases of walking (Fig. 2), with the spring stiffness experimentally determined based on structural constraints and the requirement for reliable operation at the lowest tested walking speed, assuming a practical inertial mass of 15 g. This mass can be adjusted within a practical range to accommodate variations in gait speed. Overall, this configuration balances operational stability, user comfort, and structural feasibility.

The beginning of each phase has a decelerating effect on the clutch: deceleration along the x-axis for the stance phase and deceleration along the y-axis for the swing phase, where the x- and y-axes correspond to the local coordinate frame defined by the Inertial Measurement Unit mounted on the heel of the walking boot (Fig. 2). Inertial forces induced by the decelerations are directly involved in the clutch engagement (Clutch ON) and disengagement (Clutch OFF), with the forces from the clutch springs and gravity combined (Fig. 1(*c*)). The bistable inertial clutch with the pawl gear engages a ratchet wheel around heel strike and disengages the wheel immediately after toe-off. Thus, the clutch helps the extension springs at the back of the passive-elastic ankle exoskeleton store elastic energy during ankle dorsiflexion in the stance phase and release the stored energy immediately after plantarflexion (Fig. 2). The sensitivity of the ON–OFF switching motion is directly related to the torque threshold determined by the clutch springs and can be adjusted slightly by varying the mass of the inertial weight from 2 to 15 g. To ensure clear disengagement during the switching motion even if the Clutch OFF threshold is not reached, a cylindrical pusher was installed as a mechanical booster in the clutch module to lift the bistable inertial clutch (Fig. 1). The retraction springs, which have a relatively low stiffness of 0.16 N/mm compared to the extension springs, assist in ensuring complete plantarflexion during its late stage, when the ankle reaches a more relaxed posture, thereby facilitating the effective activation of the cylindrical pusher.

The dynamic equations of motion for the bistable inertial clutch model were derived using the Newton–Euler formulation under the assumption that the collision between the pawl and ratchet gears is perfectly inelastic (Fig. 1(*c*)). The dynamic equation of the clutch model under gravity (g) is expressed as follows:

$$\begin{aligned} T_o = I_o \cdot \ddot{\theta}_c &= \underbrace{(I_w + m_w \cdot l_w^2 + I_{\text{pwl}} + m_{\text{pwl}} \cdot l_{\text{pwl}}^2) \cdot \ddot{\theta}_c}_{\text{Parallel axis theorem}} \\ &= \underbrace{-F_s \cdot l_r \cdot l_{rc}}_{\text{Clutch spring}} + \underbrace{(m_w \cdot l_w + m_{\text{pwl}} \cdot l_{\text{pwl}}) \cdot \cos\theta_c \cdot \text{ACC}_x}_{\text{Local frame translation in } x\text{-axis}} + \underbrace{(m_w \cdot l_w + m_{\text{pwl}} \cdot l_{\text{pwl}}) \cdot \sin\theta_c \cdot \text{ACC}_y}_{\text{Local frame translation in } y\text{-axis}} \\ &+ \underbrace{(m_w \cdot l_w + m_{\text{pwl}} \cdot l_{\text{pwl}}) \cdot g \cdot \sin\theta_c \cdot \cos\Theta_f + (m_w \cdot l_w + m_{\text{pwl}} \cdot l_{\text{pwl}}) \cdot g \cdot \cos\theta_c \cdot \sin\Theta_f}_{\text{Gravity}} \end{aligned} \tag{1}$$

where T_o, I_o, and $\ddot{\theta}_c$ denote the clutch joint torque, moment of inertia of the clutch about the rotational joint, and clutch angular acceleration, respectively. Other model parameters are listed in Table 1 with their corresponding values.

2.2 Clutch Optimization With Walking Data

2.2.1 Experimental Procedure. Healthy young-to-middle-age subjects (eight males, mean age: 33 ± 6 years, mean height: 173 ± 7 cm, mean body mass: 71 ± 7 kg) with no leg injuries or history of balance disorder participated in this study. The participants signed an informed consent form approved by the Institutional Review Board of the Korea Advanced Institute of Science and Technology (approval number: KH2023-081).

For data collection, all subjects were instructed to look straight ahead and walk for 1 min on a treadmill at five different speeds (0.8, 1.0, 1.2, 1.4, and 1.6 m/s) while wearing a custom-made walking boot (Fig. 3(*a*)). Each subject completed five sets of walking at the five walking speeds with a 2-min rest between each set; the order of walking speeds during each set was

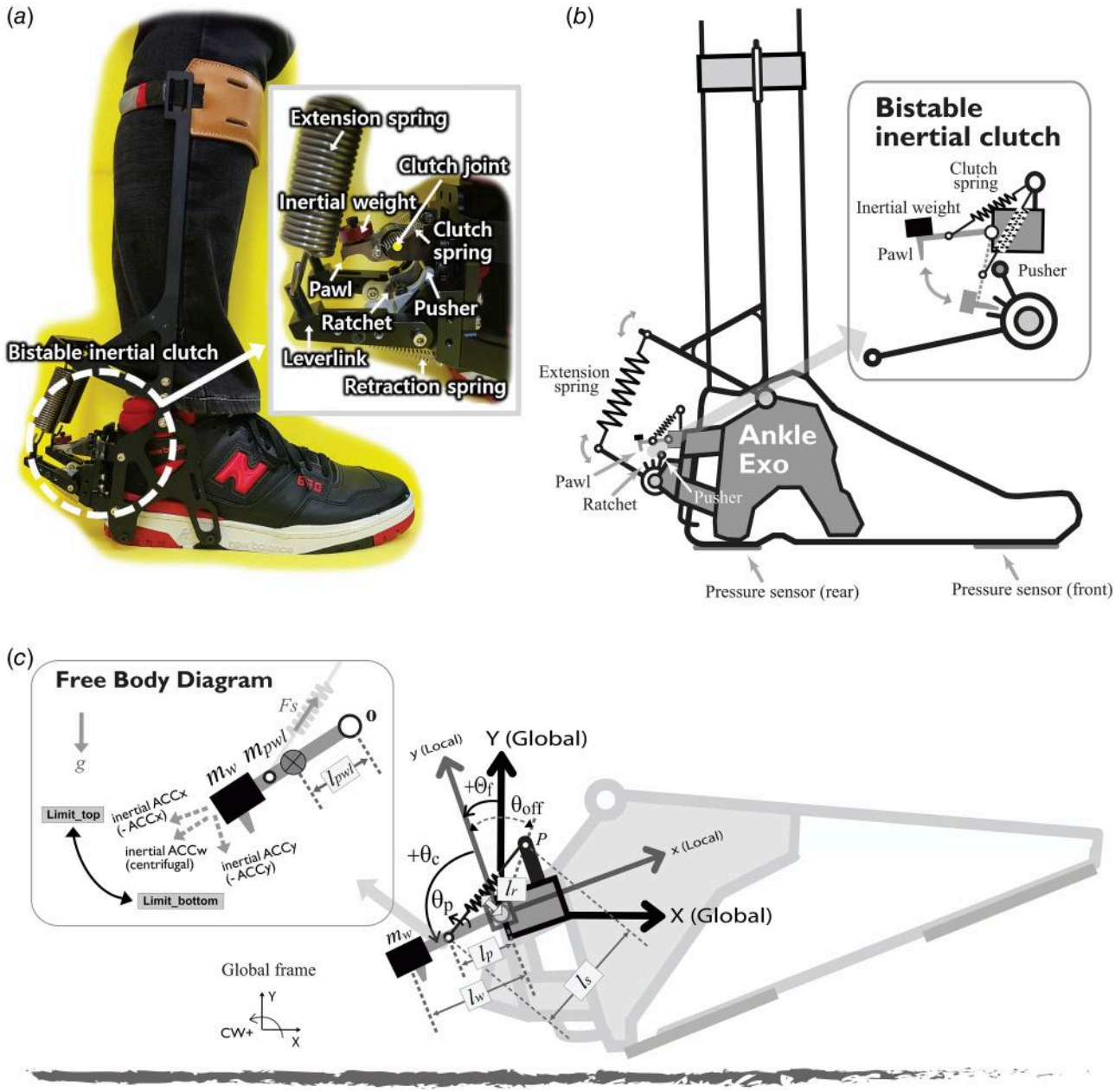

Fig. 1 Mechanical design of the bistable inertial clutch. (*a*) Photograph of the bistable inertial clutch firmly integrated into the ankle exoskeleton. (*b*) Simplified schematic that shows the stabilization of the bistable inertial clutch with respect to the clutch joint (inset). (*c*) Free body diagram of the bistable inertial clutch. All the forces acting on the masses of the inertial weight and the pawl gear are depicted with gray arrows (inset); the dashed arrows indicate inertial forces. All values of the model parameters are listed in Table 1.

random. Before data collection, the subjects participated in numerous rehearsals to become accustomed to walking while wearing the multisensor walking boot.

2.2.2 Measurements. The foot angle, heel acceleration, and foot pressure were recorded during each trial at a sampling rate of 100 Hz using the custom-made walking boot that was equipped with an inertial measurement unit and force-sensing resistors. The foot angle was measured with respect to the gravity line, and the heel accelerations were measured along the *x*- and *y*-axes with respect to the local frame, as shown in Fig. 2. Foot pressures were recorded as binary values (zero (0) and nonzero (1)) based on the threshold determined to distinguish the stance and swing phases of walking. The foot angle and heel accelerations were 5th-order Butterworth low-pass filtered with cutoff frequencies of 10 Hz for the angle data and 30 Hz for the acceleration data. The cutoff frequencies were determined via a residual analysis that decoupled white noise from the raw data by minimizing the sum of the residual error [29–33]. The simulated motion of the bistable inertial clutch (θ_c) at a given walking speed was estimated from the filtered data (Θ_f, ACC_x, ACC_y) using the dynamic equation of motion (Eq. (1)).

2.2.3 Bistable Inertial Clutch Optimization. The optimal mass of the inertial weight that enables synchronization with the stance and swing phases at a given speed was theoretically obtained using a nonlinear optimization algorithm (Sequential Quadratic Programming, Matlab®) [34–36]. The optimization was designed to minimize the least-squares error between the foot pressure data and the clutch model simulation over two sequential steps of the right

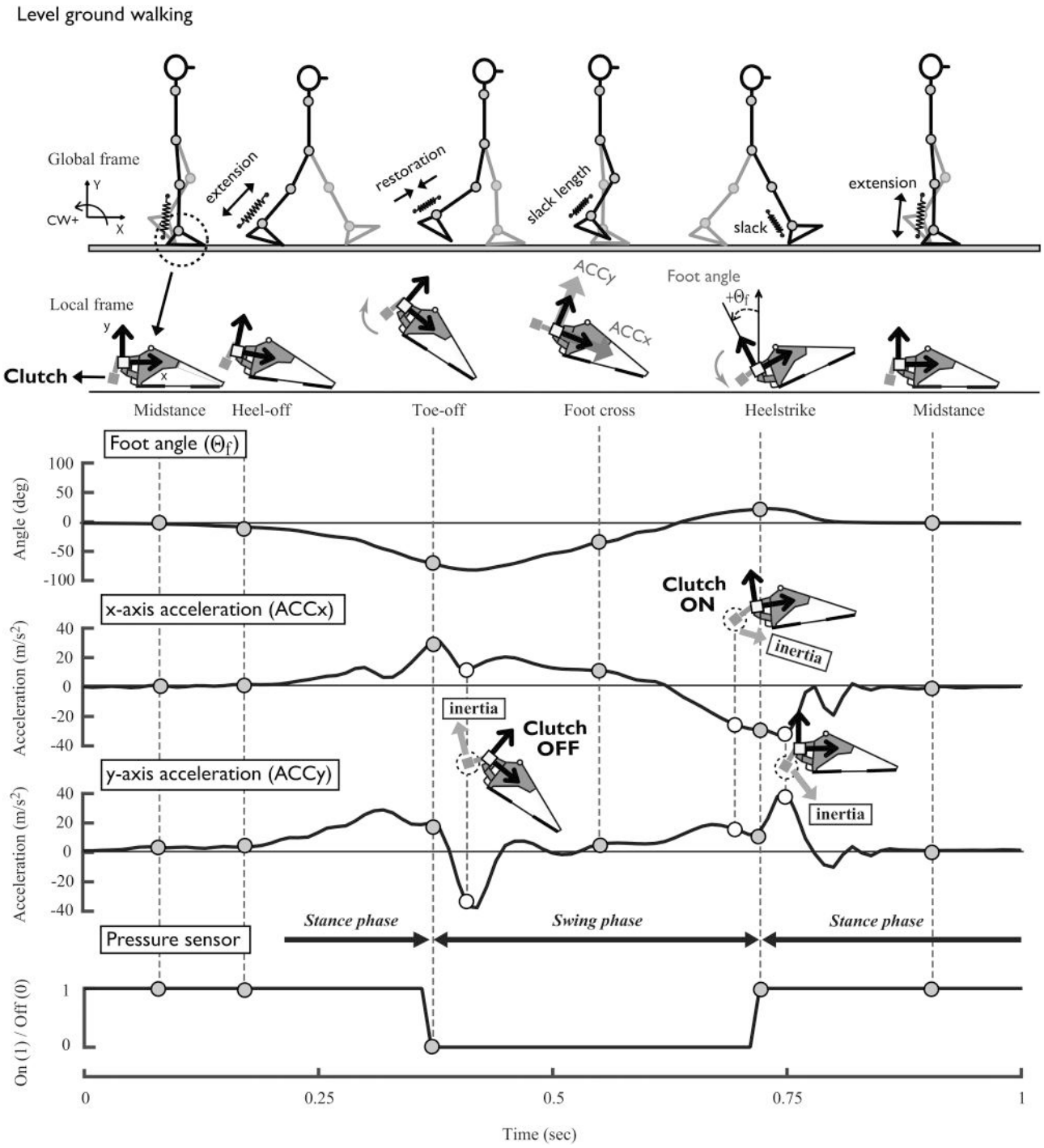

Fig. 2 Sequential action of the bistable inertial clutch during level-ground walking: the clutch engagement (Clutch ON) and disengagement (Clutch OFF) are switched based on whether or not the net torque due to the gravitational force (depending on the foot angle) and the inertial forces (induced by the clutch joint translation with respect to the global frame) exceeds the torque threshold determined by the bistable springs (see Fig. 1(c)). Considering the level of each trajectory (i.e., foot angle, *x*-axis acceleration, and *y*-axis acceleration) during walking, the clutch state is expected to change immediately before and/or after the pressure sensor value switches between zero (Clutch OFF) and nonzero (Clutch ON). Thus, the bistable inertial clutch can help extension springs store elastic energy during ankle dorsiflexion during the stance phase and release the stored energy during the following plantarflexion.

foot comprising two stance and swing phases (Fig. 4). The optimization was repeated multiple times over a wide range of random initial conditions to determine whether the solution was a global optimum. Other model parameters used in the optimization, such as the initial state and geometrical parameters, are listed in Table 1 with their corresponding values.

2.2.4 Statistical Tests of Parameter Change. The significance of the trends describing the change in parameters (e.g., kinematic data and optimal mass) as a function of the walking speed was tested using regression analysis with a significance level of $P < 0.05$. For example, once the optimal mass of the inertial weight was obtained through model simulation (based on the best-

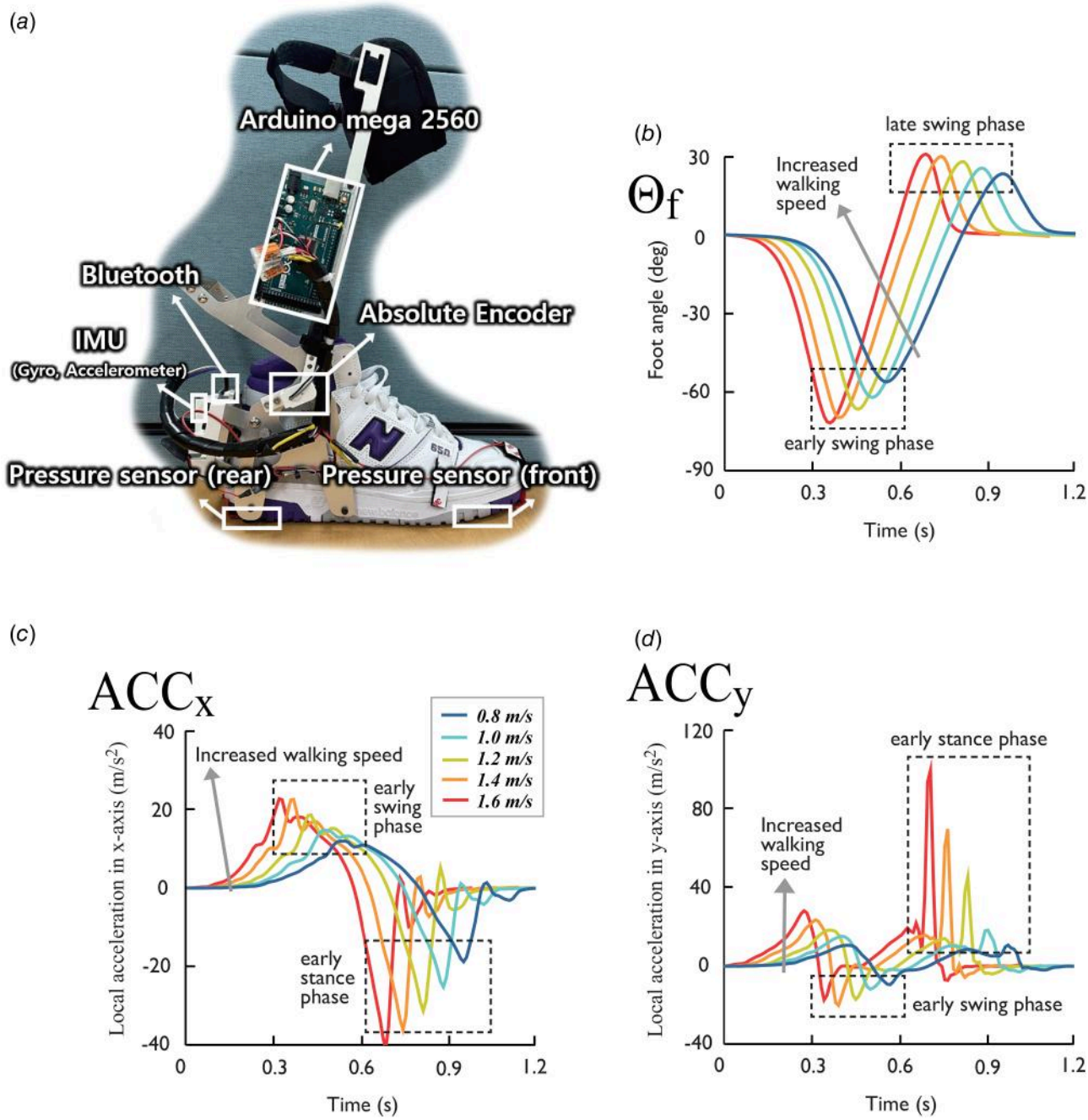

Fig. 3 Experimental data obtained from walking on a treadmill at different speeds. (*a*) Multisensor walking boot used for data collection. (*b*) Foot angle, (*c*) local acceleration along the *x*-axis, and (*d*) local acceleration along the *y*-axis, measured simultaneously using the walking boot while increasing the walking speeds (see Figs. 1(c) and 2). The data were recorded over two sequential steps between mid-stance phases; however, only one representative step is presented due to averaging, during which the foot angle and local accelerations remain approximately zero (see Fig. 2).

fitting target angle), the change in the optimal mass as a function of the walking speed was statistically tested using regression analysis with a level of significance of $P < 0.05$.

2.3 Pilot Walking Tests With the Optimal Clutch. First, five subjects (five males, mean age: 34 ± 4 years, mean height: 173 ± 7 cm, mean body mass: 76 ± 9 kg), walked on the same treadmill at incremental speeds of 0.8, 1.0, 1.2, 1.4, and 1.6 m/s while wearing the ankle exoskeleton with an optimal inertial weight at the end of the bistable inertial clutch (Fig. 1 and Table 2); the inertial weight was optimized for a walking speed of 1.2 m/s (Fig. 5), which was chosen as the nominal point to evaluate the sensitivity of the clutch mechanism to variations in walking speed using a fixed inertial mass. The treadmill speed was increased sequentially every 1 min, and the entire set was repeated twice with 5 min rest between the sets. The clutch angle and foot pressure for each trial were recorded at a sampling rate of 100 Hz, and the obtained angle data were 5th-order Butterworth low-pass filtered at a cutoff frequency of 10 Hz.

Second, the five subjects walked for 2 min on a treadmill at five different speeds (0.8, 1.0, 1.2, 1.4, and 1.6 m/s) under three conditions: (1) shoe-only, (2) exoskeleton without supportive torque, and (3) exoskeleton with supportive torque. The assisted condition

Table 1 Model parameters of the bistable inertial clutch and optimization setup

Model parameters used in optimization (refer to Fig. 1(*c*))		
Mass of inertial weight	m_w	$0.002 - 0.012$ kg
Mass of pawl gear	m_{pwl}	0.027 kg
Gravity	G	9.81 m/s^2
x-axis position of the bistable spring fixed point P	P_x	0.012 m
y-axis position of the bistable spring fixed point $\boldsymbol{P}$	P_y	0.013 m
Offset angle of the bistable spring fixed point P based on the clutch joint O	θ_{off}	$\tan^{-1}\left(\frac{P_x}{P_y}\right)$ rad
Angle between the bistable spring and pawl gear	θ_p	$\cos^{-1}\left(\frac{l_s^2 + l_p^2 - P_x^2 - P_y^2}{2 \cdot l_s \cdot l_p}\right)$ rad
Clutch angle in the local frame	θ_c	$98 - 170$ deg
Foot angle in the global frame	Θ_f	-90 to 60 deg
Length between the clutch joint O and m_w	l_w	0.02 m
Length between the clutch joint O and m_{pwl}	l_{pwl}	0.008 m
Length between the clutch joint O and the bistable spring endpoint on the pawl gear	l_p	0.009 m
Length of the bistable spring torque moment arm	l_r	$l_p \cdot \sin\theta_p m$
Sign coefficient	l_{rc}	If $\theta_{\text{off}} + \theta_c < 180°$, then 1, else -1
Slack length of the bistable spring	l_{s0}	0.015 m
Length of the bistable spring	l_s	$\sqrt{(P_x + l_p \cdot \sin\theta_c)^2 + (P_y - l_p \cdot \cos\theta_c)^2}$ m
Stiffness of the bistable spring	k_s	79.38 N/m
Initial tension of the bistable spring	F_{s0}	0.23 N
Number of the bistable spring	N_s	2
Force exerted by the bistable springs	F_s	$\{[k_s \cdot (l_s - l_0) + F_{s0}] \times N_s\}$ N
Moment of inertia about the center of mass of the corresponding weight	I_w	$(1.54 \times 10^{-3}) \cdot m_w^2 - (6.89 \times 10^{-6}) \cdot m_w + 9.24 \times 10^{-8}$ kg/m^2
Moment of inertia about the center of mass of the pawl gear	I_{pwl}	2.23×10^{-6} kg/m^2
Optimization setup		
Simulation condition		If $\theta_c \leq$ Limit_top (98 deg), set $\theta_c =$ Limit_top, $\dot{\theta}_c = 0$, $\ddot{\theta}_c = 0$ If $\theta_c \geq$ Limit_bottom (170 deg), set $\theta_c =$ Limit_bottom, $\dot{\theta}_c = 0$, $\dot{\theta}_c = 0$ Automatically Clutch OFF within 0.04 s at the start of swing phase (at pressure off)
Objective function		$F_{\text{obj}} = \min$ {RMS error between target and simulation} (refer to Fig. 4) constrained with the condition "correlation between target and simulation >0.6"

refers to walking with a passive-elastic ankle exoskeleton equipped with a bistable inertial clutch (Fig. 1(*a*)), while the unassisted condition (exoskeleton without supportive torque) indicates that the bistable inertial clutch remained disengaged (OFF) throughout walking. To generate the supportive torque, extension springs (spring constant: 2.65 N/mm; two per device) were selected to provide approximately 80–90% of the peak ankle torque reported in previous studies of older adults during walking, as a starting point for this pilot study (Fig. 6) [37]. Each subject performed two sets of walking trials, with five different speeds in each set, totaling 10 trials per condition. A rest period of 10–15 min was provided between sets. The order of walking speeds within each set was randomized. During the trials, surface electromyographic (EMG) signals were recorded from four muscle sites: medial gastrocnemius (Med. GAS), lateral gastrocnemius (Lat. GAS), upper soleus (SOL-A), and lower soleus (SOL-B) (Trigno EMG system, Delsys, USA). EMG data were sampled at 2 kHz and band-pass filtered (20–450 Hz) [38–40]. The signals were then full-wave rectified and low-pass filtered at 10 Hz to obtain the linear envelope [41]. Average muscle activation was computed as the time-averaged integral of the EMG linear envelope over the final 10 consecutive strides. To facilitate comparison, each participant's average muscle activation was normalized to the value from the shoe-only condition. This normalization accounted for inter-subject variability and allowed for relative comparisons of muscle activation across conditions [42]. A repeated-measures analysis of variance (ANOVA) was performed to compare the conditions. Post hoc comparisons were conducted using paired t-tests with Holm correction ($P < 0.05$).

3 Results

3.1 Kinematic Data Collected Using the Multisensor Walking Boot. Negative (all subjects: $P < 0.05$) and positive (four subjects: $P < 0.05$, four subjects: $P = 0.12$) peak foot angles at the beginning and end stages of the swing phase gradually increased in absolute magnitude with walking speed (Fig. 3(*b*)). The increase in the magnitude of the negative peak foot angle was attributed to greater foot pivoting during the stance phase. The increase in the positive peak foot angle suggested a larger touchdown angle around heel strike at higher walking speeds.

Positive (all subjects: $P < 0.05$) and negative (five subjects, $P < 0.05$; three subjects, $P = 0.22$) peak local accelerations along the x- and y-axes, observed during the early stage of the swing phase, increased in absolute magnitude with walking speed

Table 2 Specifications of the passive-elastic ankle exoskeleton (per leg)

Item	Material	Quantity	Unit
Exoskeleton frame with the bistable inertial clutch	Aluminum alloy 7075 and steel	550	g
Shoe (BB650, New Balance, US) + thigh pad	Leather and synthetic	540	g
Extension spring (not optimized)	Stainless steel	2	ea
Total (frame + springs + shoe + pad)		1.18	kg

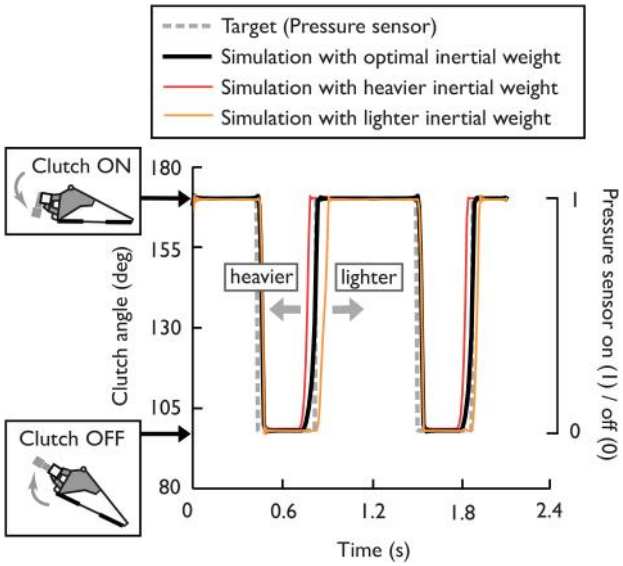

Fig. 4 Target angle for the bistable inertial clutch at a walking speed of 1.2 m/s and simulation results using different inertial weights. The trajectory of the target angle was set using signals from the foot pressure sensor (dashed gray line). The optimal inertial weight was calculated by minimizing the fitting error between the target and model simulation. The simulation results were plotted using the optimal inertial weight (thick solid line), 4 g heavier, and 1 g lighter inertial weights (thin solid lines) compared to the optimal inertial weight.

(Figs. 3(*c*) and 3(*d*)). The increase in positive peak local acceleration along the *x*-axis is attributed to the larger forward momentum generated by the larger rotational motion of the foot in a shorter time period (Fig. 3(*b*)). The increase in the magnitude of the negative peak local acceleration along the *y*-axis is attributed to the inevitable larger deceleration necessary for the subsequent forward motion of the foot.

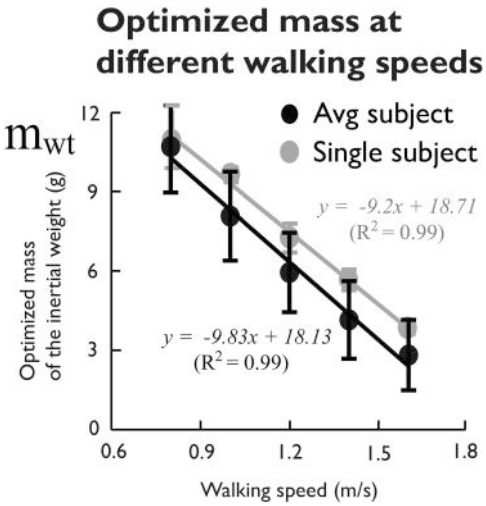

Fig. 5 Average masses of the optimal inertial weights of all subjects (black) and a single representative subject (gray) obtained via an optimization that minimizes the fitting error between the target clutch angle and the model simulation. Statistically significant gradual scaling across the walking speed was observed in both cases for the optimal inertial weight. The thick solid lines (black and gray) indicate the slopes of linear regressions of the averaged masses of the inertial weights as a function of the walking speed. The complete equations for the curve fits are displayed in the form of $y = ax + b$ along with goodness-of-fit (R^2) values. Error bars indicate standard deviation.

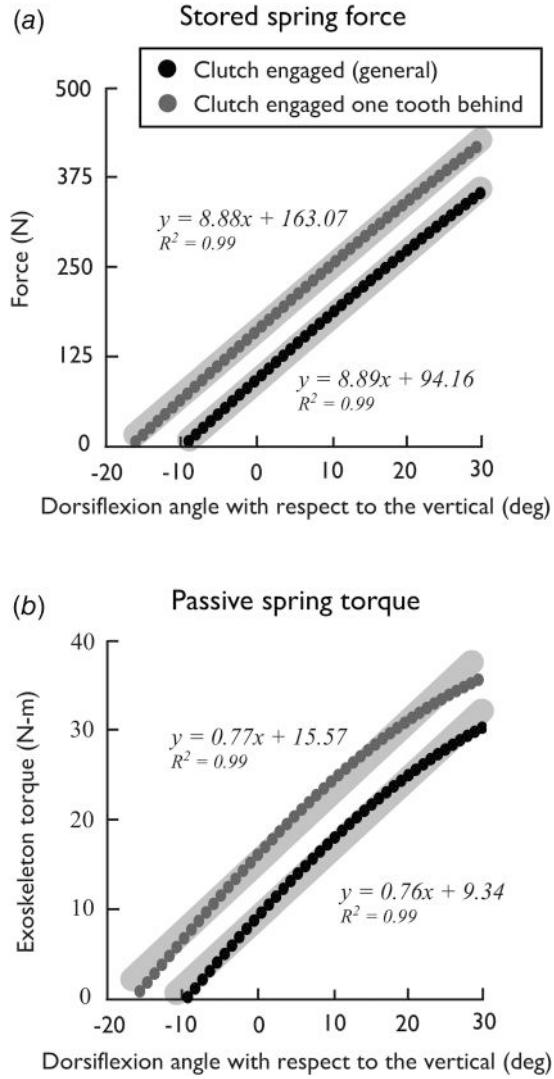

Fig. 6 (*a*) Stored spring force and (*b*) passive spring torque as a function of the dorsiflexion angle with respect to the vertical line (see Fig. 1(*b*)). Due to the negative offset angle at the onset of the ankle rocker motion, the initial force and torque exhibited positive values even when the dorsiflexion angle was zero. The elastic energy was estimated based on spring elongation inferred from ankle joint angles under quasi-static assumptions, without accounting for dynamic effects. The gray-dot line represents the condition in which the clutch engaged one tooth behind on the ratchet gear at heel strike, compared to the black-dot line. The thick, solid, light-gray lines indicate the linear regression slopes of the simulation data (dotted lines) corresponding to each value (i.e., spring force and torque, respectively) as a function of the dorsiflexion angle. The full equations for the curve fits are displayed in the form of $y = a\,x + b$ with goodness-of-fit data.

Negative (seven subjects: $P < 0.05$, 1 subject: $P = 0.13$) and positive (seven subjects: $P < 0.05$, 1 subject: $P = 0.18$) peak local accelerations along the *x*- and *y*-axes, observed during the very early stage of the stance phase, increased in absolute magnitude with walking speed (Figs. 3(*c*) and 3(*d*)). The increase in the magnitude of the peak values is attributed to the increased momentum of the center of mass (CoM). Because the direction of CoM momentum must change during the step-to-step transition (i.e., stance phase) to maintain a steady gait with increasing speed [43–45], the heel accelerations during the early stance phase along both the *x*- and *y*-axes are naturally larger owing to physical collisions between the foot and ground (i.e., heel strike) [46].

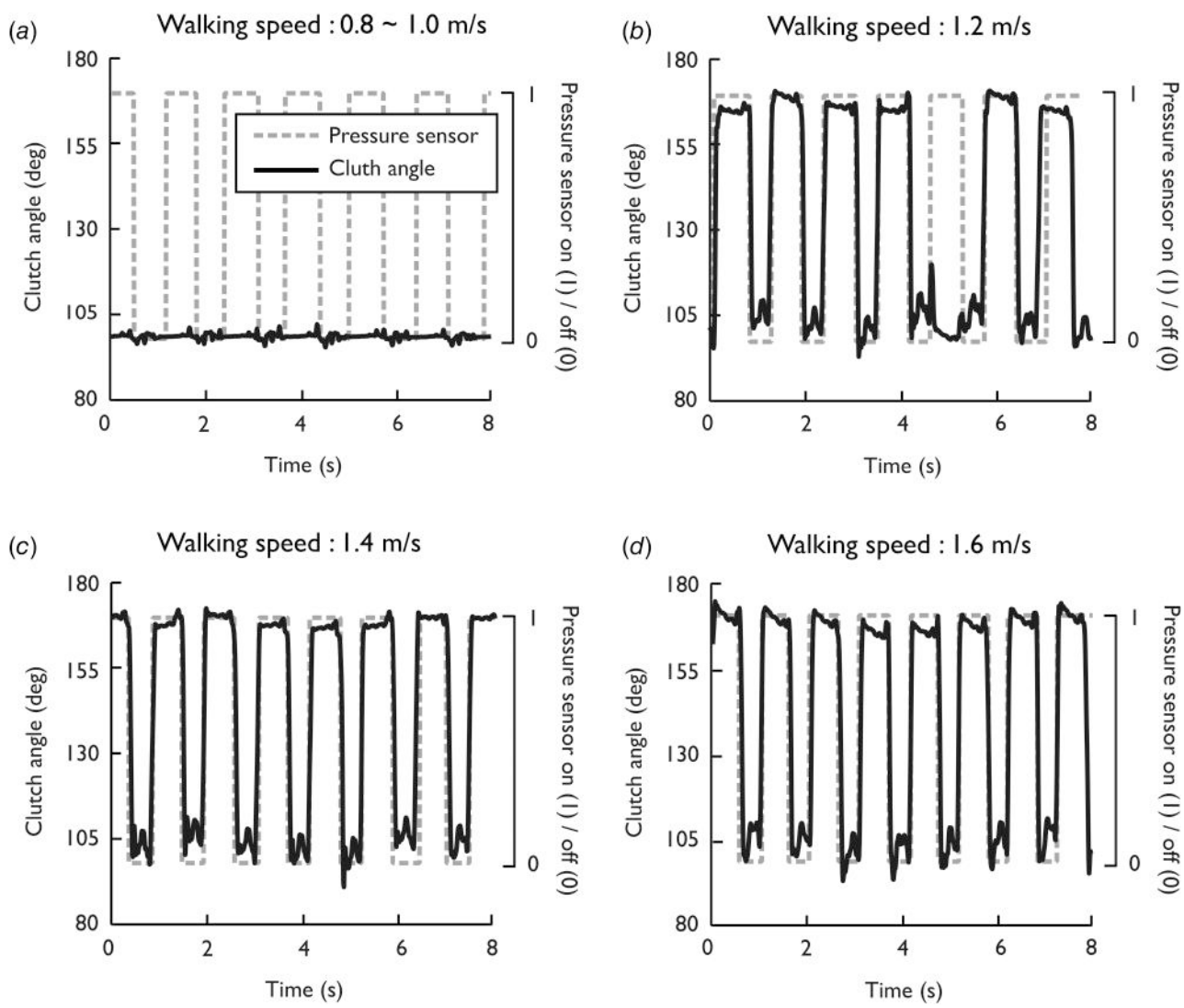

Fig. 7 Bistable inertial clutch angle and pressure on/off value obtained from walking on a treadmill at different speeds. After adding a near-optimal inertial weight of 7 g (corresponding to a walking speed = 1.2 m/s) to the bistable inertial clutch, the representative subject (see Fig. 5) wearing the passive-elastic ankle exoskeleton walked on the treadmill at the speeds of (*a*) 0.8–1.0, (*b*) 1.2, (*c*) 1.4, and (*d*) 1.6 m/s, respectively. The action of the bistable inertial clutch began after the treadmill speed exceeded (*b*) 1.2 m/s. Nonworking trials were significantly reduced at the speeds of (*c*) 1.4 and (*d*) 1.6 m/s. The fluctuation in the time-series data around the limit angles of the bistable inertial clutch was due to the behavior of the clutch springs that prevented transition between the states.

3.2 Optimized Inertial Weights for Different Walking Speeds. The theoretically calculated optimal mass of the inertial weight obtained from model simulation (based on the best-fitting target angle) gradually decreased with an increase in the walking speed ($P < 0.05$) (Figs. 4 and 5). The average mass of the inertial weight of all the subjects ($N = 8$), obtained by minimizing the fitting error between the target clutch angle and the model simulation, was gradually scaled across the walking speeds with a coefficient of determination of $R^2 = 0.99$; the inertial weight of each subject showed a similar scaling trend with increasing speed (Fig. 5). Optimal masses of the inertial weight for all subjects across different walking speeds were predicted to be less than 15 g.

3.3 Operation of the Bistable Inertial Clutch at Different Walking Speeds. The bistable inertial clutch with the optimal inertial weight corresponding to a walking speed of 1.2 m/s started switching between the Clutch ON and OFF states after the treadmill speed exceeded 1.2 m/s. In particular, nonworking trials were significantly reduced at the speeds of 1.4 and 1.6 m/s, as predicted (Fig. 7). A clear disengagement (Clutch OFF) from the previous engagement (Clutch ON) was guaranteed at all walking speeds because the mechanical pusher acted as a mechanical booster to lift the clutch. The fluctuations in the time-series data around the limit angles of the bistable inertial clutch were attributed to the behavior of the clutch springs, which prevented transition between the states in case the threshold is not reached; the fluctuations were clearly evident at a speed of 1.6 m/s.

3.4 Electromyographic Data Collected Under Different Walking Conditions. Across all walking speeds and muscles, the exoskeleton without supportive torque condition showed the highest average muscle activation values, while the exoskeleton

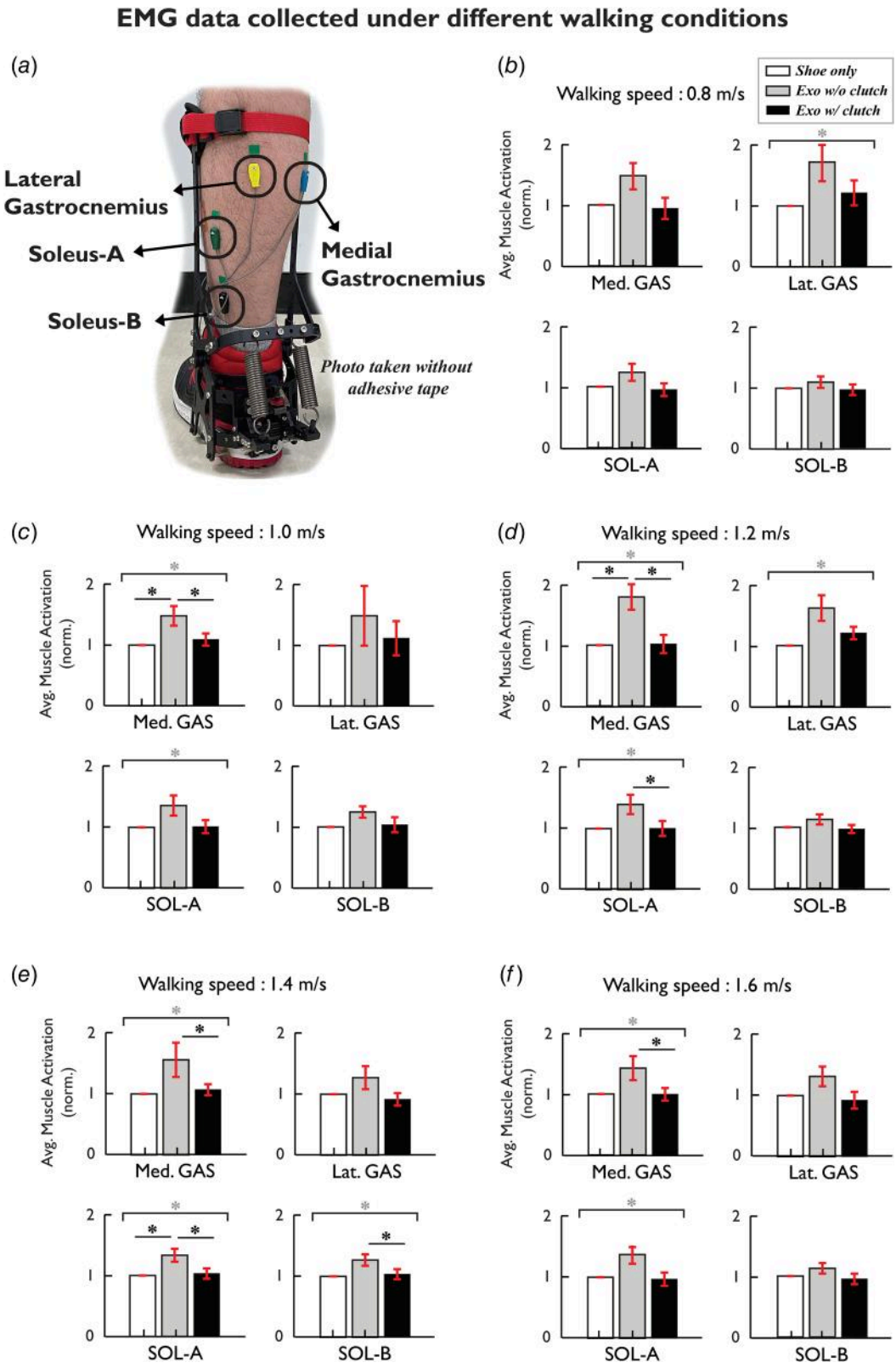

Fig. 8 (*a*) Electrode placement for surface EMG measurement. EMG data collected under different walking conditions at each walking speed: 0.8 (*b*), 1.0 (*c*), 1.2 (*d*), 1.4 (*e*), and 1.6 m/s (*f*). Mean and standard error of average muscle activation values of EMG signals calculated over the final 10 consecutive strides of walking under three conditions: shoe only (white bar), exoskeleton without supportive torque (gray bar), and exoskeleton with supportive torque (black bar). Values were normalized to the "shoe-only" condition for better comparison. The exoskeleton with supportive torque represents the assisted condition, whereas the exoskeleton without supportive torque indicates that the bistable inertial clutch remained OFF throughout walking. Gray asterisks (*) indicate significant main effects from repeated-measures ANOVA ($P < 0.05$), while black asterisks (*) denote significant pairwise differences from Holm-corrected post hoc tests ($P < 0.05$).

with supportive torque condition showed similar values to the shoe only condition, with no statistical differences (Fig. 8). At a walking speed of 0.8 m/s, repeated-measures ANOVA revealed a significant difference only in Lat. GAS; however, post hoc tests did not detect any significant pairwise differences (Fig. 8(*b*)). At 1.0 m/s, significant differences were found in Med. GAS and SOL-A. Post hoc tests showed significant pairwise differences in Med. GAS between the shoe only and exoskeleton without supportive torque conditions, as well as between the two exoskeleton conditions. No significant pairwise differences were found in SOL-A (Fig. 8(*c*)). At 1.2 m/s, significant differences were observed in Med. GAS, Lat. GAS, and SOL-A. Post hoc tests revealed significant differences in Med. GAS between the shoe only and exoskeleton without supportive torque conditions, and between the two exoskeleton conditions. In SOL-A, a significant difference was observed between the two exoskeleton conditions, while no significant pairwise differences were found in Lat. GAS (Fig. 8(*d*)). At 1.4 m/s, significant differences were found in Med. GAS, SOL-A, and SOL-B. Post hoc tests showed significant pairwise differences in Med. GAS between the two exoskeleton conditions; in SOL-A, between the shoe only and exoskeleton without supportive torque conditions, as well as between the two exoskeleton conditions; and in SOL-B, between the two exoskeleton conditions (Fig. 8(*e*)). At 1.6 m/s, significant differences were found in Med. GAS and SOL-A. Post hoc tests revealed a significant pairwise difference in Med. GAS between the two exoskeleton conditions, whereas no significant differences were found in SOL-A (Fig. 8(*f*)).

4 Discussion

4.1 Increasing Inertial Forces With Increasing Walking Speed Requires Less Added Mass to Overcome the Threshold for the Clutch Action. Based on the walking data, the bistable inertial clutch was designed to switch between the Clutch ON and OFF states in a timely manner during the stance and swing phases of walking, respectively (Figs. 2 and 3). The direction of heel acceleration at the clutch joint changes during both the initial and later parts of the swing phase, as reflected primarily by changes in the signs of the accelerations along the *x*-axis (e.g., later half of the swing phase) and *y*-axis (e.g., initial part of the swing phase). After the sign changes, the absolute magnitude of heel acceleration gradually increases due to the swing foot trajectory and ground collision, eventually reaching a level that allows the bistable inertial clutch to overcome the switching threshold set by two passive clutch springs. Furthermore, peak accelerations during both the early swing and early stance phases increase with walking speed (Figs. 3(*c*) and 3(*d*)). These peak accelerations generate inertial forces that result in a larger switching torque on the inertial weight of the clutch. As a result of the larger inertial forces, the optimal mass of the inertial weight naturally decreases with increasing walking speed (Fig. 5).

For instance, the model simulation indicated that, with a heavier inertial weight than the optimal inertial weight, the clutch switching from the disengagement state (Clutch OFF) starts earlier and ends before entering the stance phase owing to the larger inertial forces due to the heavier mass. In contrast, with a lighter inertial weight, the clutch switching starts after entering the stance phase, indicating that a heel strike is necessary for triggering the clutch action (Fig. 4). In addition, at identical inertial weights, the success rate of clutch switching increased with an increase in the walking speed (Fig. 7), as predicted from the clutch dynamics (Eq. (1)). This suggests that once an inertial weight is determined for a given speed, it could also be applied to higher speeds.

From the perspective of energy utilization, the proposed bistable inertial clutch allows elastic energy to be stored continuously throughout the ankle rocker phase, unlike conventional passive clutches that operate at fixed timings after heel strike or during part of the ankle rocker. These prior mechanisms are limited in their ability to store energy effectively. In contrast, our clutch synchronizes with walking dynamics, enabling more efficient energy capture and phase-aligned release.

4.2 Mechanical Pusher Helps to Easily Lift Up the Bistable Inertial Clutch Despite Not Reaching the Threshold for the Clutch OFF. Heel accelerations during the early swing phase are often insufficient for clutch disengagement. In particular, the peak amplitudes of the accelerations during the early swing phase are smaller than those during the late swing or early stance phases (Figs. 3(*c*) and 3(*d*)). Moreover, the gravitational torque is inherently disadvantageous to clutch disengagement (Clutch OFF) because it acts along the opposite direction. Hence, a mechanical pusher was added to the clutch module to ensure clear disengagement (Clutch OFF).

The bistable inertial clutch can function without the booster. However, a pusher compensates for the discrepancies between the levels of peak accelerations during the two walking phases and, thus, facilitates synchronous clutch operation during the stance and swing phases. Therefore, the optimal mass of the clutch was also calculated theoretically under the simulation condition that the clutch is automatically disengaged within 0.04 s from the beginning of the swing phase.

4.3 Passive-Elastic Ankle Exoskeleton Requires Careful Design for Effective Performance. The first prototype of the ankle exoskeleton with the bistable inertial clutch demonstrated robust control of extension spring force transmission during walking. However, performance evaluation based on muscle activation indicates that further improvements require a better design with optimized springs. The stiffness of the current extension springs, used as a starting point in this pilot study, was similar to or slightly lower than that of springs designed for older adults in previous literature [37] and was not optimized for each individual healthy subject in this study. The frame mass in this prototype may also need to be reduced by approximately 50–100 g compared to exoskeletons successfully demonstrated in prior studies [13]. If these factors are improved, the reduction in muscle activation currently observed primarily between the exoskeleton without supportive torque and the exoskeleton with supportive torque conditions may also be observed between the shoe only and the exoskeleton with supportive torque conditions (Fig. 8). It is expected that a simpler and lighter design, combined with optimized stiffness, could lead to improved performance evaluation.

4.4 Sensitivity Analysis Suggests Applicability to Various Walking Environments. A simulation-based sensitivity analysis suggests that the clutch can maintain stable ON–OFF switching performance under kinematic variations (e.g., heel acceleration and foot angle magnitudes) representative of uneven terrain, step variability, and small disturbances (Figs. 9 and 10). An inertial weight optimized for a specific walking speed enabled the bistable inertial clutch mechanism to operate normally under increased heel accelerations and/or foot angles. However, the clutch showed difficulty in triggering ON–OFF switching when heel accelerations significantly decreased, particularly at walking speeds below 1.2 m/s, as observed in the sensitivity analysis involving both single (Fig. 9) and dual (Fig. 10) parameter changes. These results indicate that once the inertial weight is optimized for a given speed, the clutch is robust to small disturbances and may also be applicable to higher walking speeds.

The clutch may also operate stably during mildly inclined walking conditions. During downhill walking, the maximum plantarflexion angle at heel strike naturally increases [47]. Although this variation does not pose a direct threat to the clutch mechanism, as supported by the sensitivity analysis on foot angle, it may affect the timing of clutch engagement. This is because the altered foot

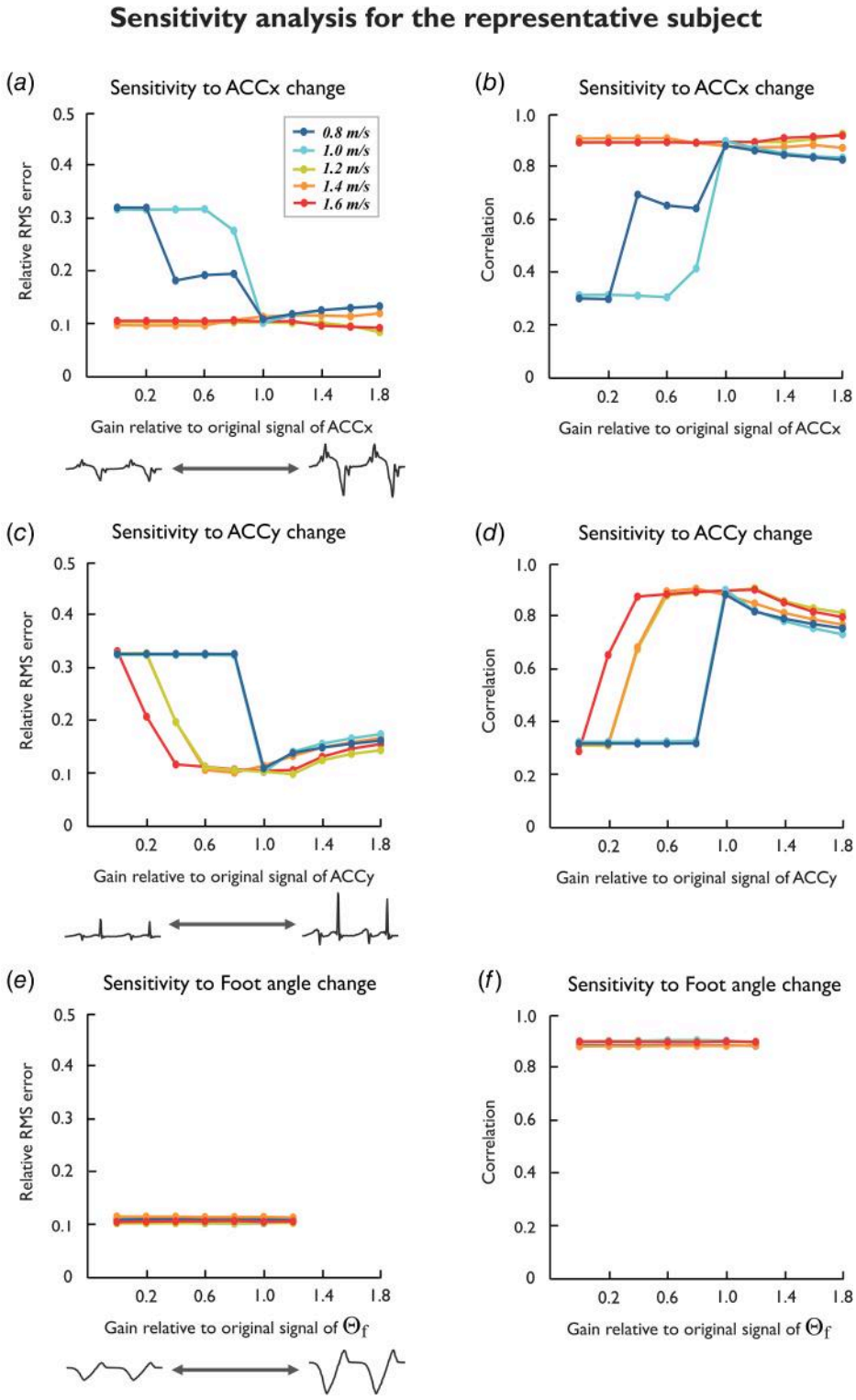

Fig. 9 Sensitivity analysis based on dynamic simulation by varying a single parameter. Heel accelerations along the *x*-axis (*a* and *b*), heel accelerations along the *y*-axis (*c* and *d*), and foot angles obtained from the walking experiment (*e* and *f*) were scaled in amplitude by adjusting the gain relative to their original values, ranging from smaller to larger values. For each case, the root mean square (RMS) errors (*a*, *c*, and *e*) and correlation coefficients (*b*, *d*, and *f*) between the reference and simulated clutch profiles are presented as a function of the gain.

angle, and consequently the position of the pusher at the moment of engagement, can influence when engagement occurs. To address this, the clutch design incorporates an inherent gravitational fail-safe, enabled by the bistable mechanism, which functions reliably under moderate walking speeds and gentle slopes. Even if the pusher mechanism temporarily delays engagement at heel strike, the slight dorsiflexion that naturally follows as the foot flattens can realign the mechanism. In such cases, gravity assists the pawl in rotating downward, enabling secure engagement with the ratchet wheel.

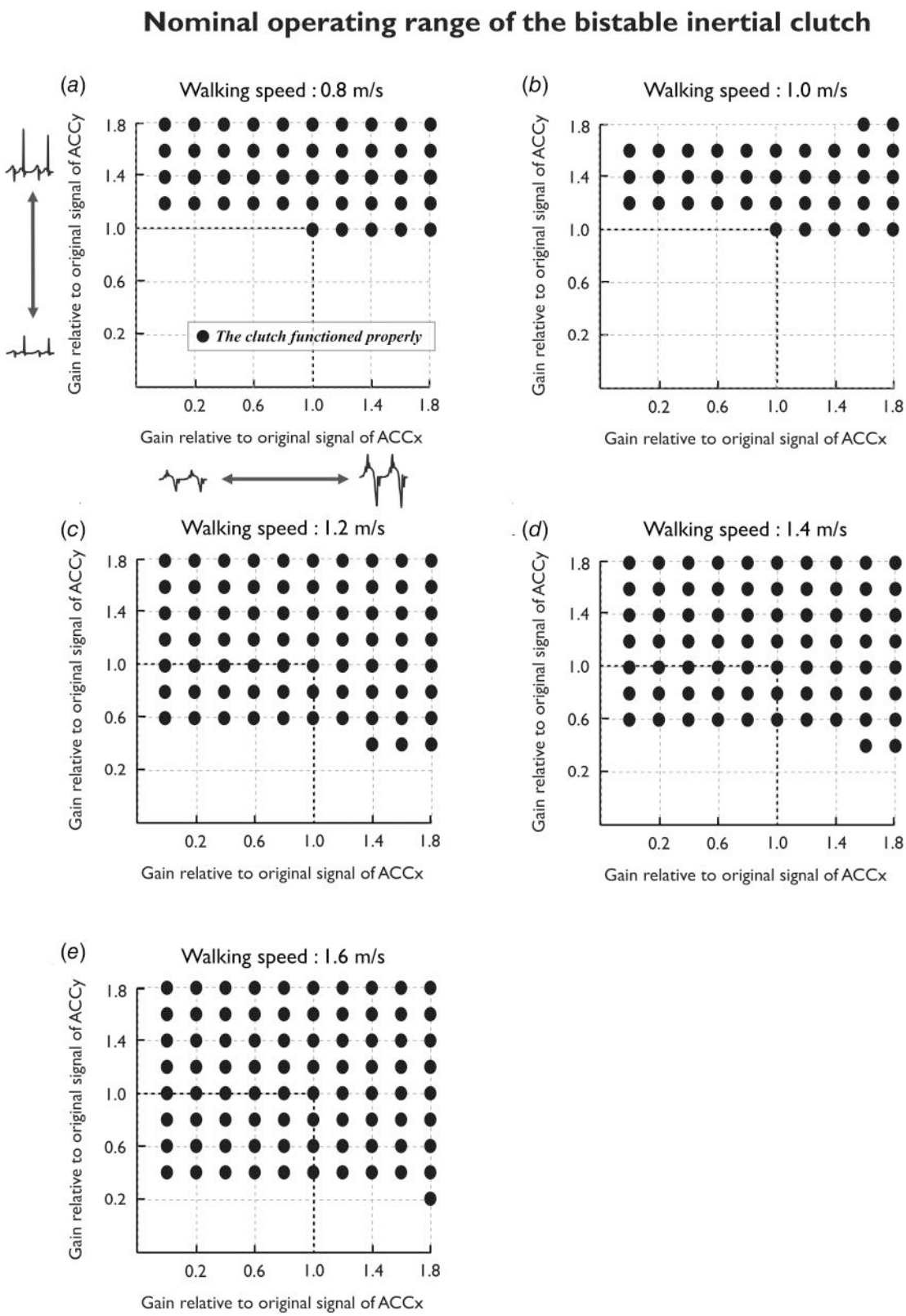

Fig. 10 Sensitivity analysis using dynamic simulation by jointly varying *x*- and *y*-axis heel accelerations. Gains were adjusted relative to original values at walking speeds of 0.8–1.6 m/s (*a*–*e*). Black circles indicate trials where the clutch functioned properly.

4.5 Future Works. The switching function of a mechanical clutch is essential for the timely storage and release of elastic energy from the extension springs installed on the ankle exoskeleton. In this study, we focused on the design (Fig. 1) of a bistable inertial clutch that can operate synchronously with the stance and swing phases of walking. The optimal inertial weight at a given walking speed was theoretically calculated. In future work, we intend to determine the optimal stiffness of the extension spring

that provides assistive ankle torque to help individuals walk efficiently across various walking speeds and conditions. Although the passive-elastic ankle exoskeleton did not demonstrate improved performance in terms of muscle activation, as measured by EMG, compared to the unassisted (i.e., shoe-only) condition, we expect that a simpler and lighter design, combined with optimized stiffness, could lead to improved outcomes.

Acknowledgment

This work was supported by the National Research Foundation of Korea (NRF) grant funded by the Korean Government (MSIT) (Grant No. NRF-2022M3C1A3080598). The authors thank Kwangjoon Kim and Joochan Lee for their contributions to data collection.

Conflict of Interest

There are no conflicts of interest.

Data Availability Statement

The datasets generated and supporting the findings of this article are obtainable from the corresponding author upon reasonable request.

References

[1] Galle, S., Malcolm, P., Collins, S. H., and De Clercq, D., 2017, "Reducing the Metabolic Cost of Walking With an Ankle Exoskeleton: Interaction Between Actuation Timing and Power," J. NeuroEng. Rehabil., **14**(35), pp. 1–16.

[2] Malcolm, P., Derave, W., Galle, S., and De Clercq, D., 2013, "A Simple Exoskeleton That Assists Plantarflexion Can Reduce the Metabolic Cost of Human Walking," PLoS One, **8**(2), p. e56137.

[3] Grimmer, M., Quinlivan, B. T., Lee, S., Malcolm, P., Rossi, D. M., Siviy, C., and Walsh, C. J., 2019, "Comparison of the Human-Exosuit Interaction Using Ankle Moment and Ankle Positive Power Inspired Walking Assistance," J. Biomech., **83**, pp. 76–84.

[4] Zhang, J., Fiers, P., Witte, K. A., Jackson, R. W., Poggensee, K. L., Atkeson, C. G., and Collins, S. H., 2017, "Human-in-the-Loop Optimization of Exoskeleton Assistance During Walking," Science, **356**(6344), pp. 1280–1284.

[5] Dijk, W. v., Meijneke, C., and Kooij, H. v. d., 2017, "Evaluation of the Achilles Ankle Exoskeleton," IEEE Trans. Neural Syst. Rehabil. Eng., **25**(2), pp. 151–160.

[6] Mooney, L. M., Rouse, E. J., and Herr, H. M., 2014, "Autonomous Exoskeleton Reduces Metabolic Cost of Human Walking During Load Carriage," J. NeuroEng. Rehabil., **11**(80), pp. 1–11.

[7] Meijneke, C., Dijk, W. v., and Kooij, H. v. d., 2014, "Achilles: An Autonomous Lightweight Ankle Exoskeleton to Provide Push-Off Power," Proceedings of the Fifth IEEE RAS/EMBS International Conference on Biomedical Robotics and Biomechatronics, Sao Paulo, Brazil, Aug. 12–15, pp. 918–923.

[8] Awad, L. N., Bae, J., O'Donnell, K., De Rossi, S. M. M., Hendron, K., Sloot, L. H., Kudzia, P., et al., 2017, "A Soft Robotic Exosuit Improves Walking in Patients After Stroke," Sci. Transl. Med., **9**(400), p. eaai9084.

[9] Kim, S., Son, Y., Choi, S., Ham, S., and Park, C., 2015, "Design of a Simple, Lightweight, Passive-Elastic Ankle Exoskeleton Supporting Ankle Joint Stiffness," Rev. Sci. Instrum., **86**(9), p. 095107.

[10] Yandell, M. B., Tacca, J. R., and Zelik, K. E., 2019, "Design of a Low Profile, Unpowered Ankle Exoskeleton That Fits Under Clothes: Overcoming Practical Barriers to Widespread Societal Adoption," IEEE Trans. Neural Syst. Rehabil. Eng., **27**(4), pp. 712–723.

[11] Quinto, L. F. P., Pinheiro, P., Gonçalves, S., Ferreira, R., Roupa, I., and da Silva, M. T., 2022, "Development and Functional Evaluation of a Passive Ankle Exoskeleton to Support Military Locomotion," Adv. Mil. Technol., **17**(1), pp. 79–95.

[12] Sawicki, G. S., Beck, O. N., Kang, I., and Young, A. J., 2020, "The Exoskeleton Expansion: Improving Walking and Running Economy," J. NeuroEng. Rehabil., **17**(25), pp. 1–9.

[13] Collins, S. H., Wiggin, M. B., and Sawicki, G. S., 2015, "Reducing the Energy Cost of Human Walking Using an Unpowered Exoskeleton," Nature, **522**(7555), pp. 212–215.

[14] Xu, S., Tang, K., Xu, L., and Ding, Y., 2025, "Design, Analysis, and Validation of a Passive Parallel Continuum Ankle Exoskeleton for Support and Walking Assistance," ASME J. Mech. Rob., **17**(3), p. 031003.

[15] Song, Q., Zhou, N., Liu, Y., and Deng, H., 2023, "The Effect of Walking With Elastic Ankle Exoskeletons on the Internal Force of Knee and Ankle," Adv. Rob., **37**(14), pp. 913–923.

[16] Farris, D. J., and Sawicki, G. S., 2012, "Linking the Mechanics and Energetics of Hopping With Elastic Ankle Exoskeletons," J. Appl. Physiol., **113**(12), pp. 1862–1872.

[17] Farris, D. J., Po, J. C. N., Yee, J., Williamson, J. L., and Dick, T. J. M., 2024, "Effects of Passive Ankle Exoskeletons on Neuromuscular Function During Exaggerated Standing Sway," R. Soc. Open Sci., **11**(5), p. 230590.

[18] Wiggin, M. B., Sawicki, G. S., and Collins, S. H., 2011, "An Exoskeleton Using Controlled Energy Storage and Release to Aid Ankle Propulsion," IEEE Interntional Conference on Rehabilitation Robotics, Zurich, Switzerland, June 29–July 1, pp. 1–5.

[19] Pardoel, S., and Doumit, M., 2019, "Development and Testing of a Passive Ankle Exoskeleton," Biocybern. Biomed. Eng., **39**(3), pp. 902–913.

[20] Hu, D., Xiong, C., Wang, T., Zhou, T., Liang, J., and Li, Y., 2022, "Modulating Energy Among Foot-Ankle Complex With an Unpowered Exoskeleton Improves Human Walking Economy," IEEE Trans. Neural Syst. Rehabil. Eng., **30**, pp. 1961–1970.

[21] Kumar, S., Zwall, M. R., Bolívar-Nieto, E. A., Gregg, R. D., and Gans, N., 2020, "Extremum Seeking Control for Stiffness Auto-Tuning of a Quasi-Passive Ankle Exoskeleton," IEEE Rob. Autom. Lett., **5**(3), pp. 4604–4611.

[22] Diller, S., Majidi, C., and Collins, S. H., "A Lightweight, Low-Power Electroadhesive Clutch and Spring for Exoskeleton Actuation," Proceedings of the 2016 IEEE International Conference on Robotics and Automation (ICRA), Stockholm, Sweden, May 16–21, pp. 682–689.

[23] Collins, S. H., and Kuo, A. D., 2010, "Recycling Energy to Restore Impaired Ankle Function During Human Walking," PLoS One, **5**(2), p. e9307.

[24] Wang, X., Guo, S., Qu, H., and Song, M., 2019, "Design of a Purely Mechanical Sensor-Controller Integrated System for Walking Assistance on an Ankle-Foot Exoskeleton," Sensors (Basel), **19**(14), p. 3196.

[25] Wang, X., Guo, S., Qu, B., Song, M., and Qu, H., 2020, "Design of a Passive Gait-Based Ankle-Foot Exoskeleton With Self-Adaptive Capability," Chin. J. Mech. Eng., **33**(49), pp. 1–11.

[26] Etenzi, E., Borzuola, R., and Grabowski, A. M., 2020, "Passive-Elastic Knee-Ankle Exoskeleton Reduces the Metabolic Cost of Walking," J. NeuroEng. Rehabil., **17**(104), pp. 1–15.

[27] Machens, K.-U. J., Neumann, J., Scholz, J., and Markiewicz, M., 2017, "Ball Sensor Rattle: Experimental and Numerical Sensitivity Study for Seatbelt Applications," Proc. Meet. Acoust., **30**(1), p. 065002.

[28] Soica, A., and Gheorghe, C., 2025, "A Review of Seatbelt Technologies and Their Role in Vehicle Safety," Appl. Sci., **15**(10), p. 5303.

[29] Burkhart, T. A., Dunning, C. E., and Andrews, D. M., 2011, "Determining the Optimal System-Specific Cut-Off Frequencies for Filtering In-Vitro Upper Extremity Impact Force and Acceleration Data by Residual Analysis," J. Biomech., **44**(15), pp. 2728–2731.

[30] Fekete, T., Rubin, D., Carlson, J. M., and Mujica-Parodi, L. R., 2011, "The NIRS Analysis Package: Noise Reduction and Statistical Inference," PLoS One, **6**(9), p. e24322.

[31] Salavati, M., Hadian, M. R., Mazaheri, M., Negahban, H., Ebrahimi, I., Talebian, S., Jafari, A. H., Sanjari, M. A., Sohani, S. M., and Parnianpour, M., 2009, "Test–Retest Reliabty of Center of Pressure Measures of Postural Stability During Quiet Standing in a Group With Musculoskeletal Disorders Consisting of Low Back Pain, Anterior Cruciate Ligament Injury and Functional Ankle Instability," Gait Posture, **29**(3), pp. 460–464.

[32] Sinclair, J., Taylor, P. J., and Hobbs, S. J., 2013, "Digital Filtering of Three-Dimensional Lower Extremity Kinematics: An Assessment," J. Hum. Kinet., **39**(1), pp. 25–36.

[33] Kim, S., Park, C., and Park, C., 2020, "Change in Telescoping Leg Strategy With Varying Walking Speed to Modulate Force Advantage," J. Theor. Biol., **496**, p. 110249.

[34] Kim, S., and Park, S., 2011, "Leg Stiffness Increases With Speed to Modulate Gait Frequency and Propulsion Energy," J. Biomech., **44**(7), pp. 1253–1258.

[35] Kim, S., Atkeson, C. G., and Park, S., 2012, "Perturbation-Dependent Selection of Postural Feedback Gain and Its Scaling," J. Biomech., **45**(8), pp. 1379–1386.

[36] Keren, R., and Or, Y., 2018, "Theoretical Analysis and Numerical Optimization of a Wearable Spring-Clutch Mechanism for Reducing Metabolic Energy Cost During Human Walking," ASME J. Mech. Rob., **10**(6), p. 061004.

[37] Lakmazaheri, A., Song, S., Vuong, B. B., Biskner, B., Kado, D. M., and Collins, S. H., 2024, "Optimizing Exoskeleton Assistance to Improve Walking Speed and Energy Economy for Older Adults," J. NeuroEng. Rehabil., **21**(1), pp. 1–14.

[38] Ishibashi, K., Yoshikawa, K., Koseki, K., Aoyama, T., Ishii, D., Yamamoto, S., Matsuda, T., Tomita, K., Mutsuzaki, H., and Kohno, Y., 2021, "Gait Training After Stroke With a Wearable Robotic Device: A Case Report of Further Improvements in Walking Ability After a Recovery Plateau," Prog. Rehabil. Med., **6**(37), pp. 1–13.

[39] Ebihara, A., Hirota, M., Kumakura, Y., and Nagaoka, M., 2023, "Analysis of Muscle Synergy and Gait Kinematics During Regain of Gait Function Through Rehabilitation in a Monoplegic Patient," Front. Hum. Neurosci., **17**, pp. 1–18.

[40] Hellman, E., Arokoski, J., Franz, J., Andersen, M. S., Korhonen, R. K., and Stenroth, L., 2025, "Acute Effects of Soleus EMG Biofeedback Training on Tibiofemoral Joint Contact Forces in Young Healthy Adults," J. Biomech., **184**, p. 112646.

[41] Nuckols, R. W., and Sawicki, G. S., 2020, "Impact of Elastic Ankle Exoskeleton Stiffness on Neuromechanics and Energetics of Human Walking Across Multiple Speeds," J. Neuroeng. Rehabil., **17**(75), pp. 1–19.

[42] Hybart, R. L., and Ferris, D. P., 2023, "Neuromechanical Adaptation to Walking With Electromechanical Ankle Exoskeletons Under Proportional Myoelectric Control," IEEE Open J. Eng. Med. Biol., **4**, pp. 119–128.
[43] Donelan, J. M., Kram, R., and Kuo, A. D., 2002, "Mechanical Work for Step-to-Step Transitions Is a Major Determinant of the Metabolic Cost of Human Walking," J. Exp. Biol., **205**(Pt 23), pp. 3717–3727.
[44] Adamczyk, P. G., and Kuo, A. D., 2009, "Redirection of Center-of-Mass Velocity During the Step-to-Step Transition of Human Walking," J. Exp. Biol., **212**(Pt 16), pp. 2668–2678.
[45] Kim, S., and Park, S., 2012, "The Oscillatory Behavior of the CoM Facilitates Mechanical Energy Balance Between Push-Off and Heel Strike," J. Biomech., **45**(2), pp. 326–333.
[46] Baines, P. M., Schwab, A. L., and van Soest, A. J., 2018, "Experimental Estimation of Energy Absorption During Heel Strike in Human Barefoot Walking," PLoS One, **13**(6), p. e0197428.
[47] Montgomery, J. R., and Grabowski, A. M., 2018, "The Contributions of Ankle, Knee and Hip Joint Work to Individual Leg Work Change During Uphill and Downhill Walking Over a Range of Speeds," R. Soc. Open Sci., **5**(8), p. 180550.